A DFT Study of Pt Particles Growth inside β-Zeolite Cages

Laura Gueci, Marco Bertini, Chiara Nania, Francesco Ferrante,* and Dario Duca

Dipartimento di Fisica e Chimica "Emilio Segrè", Università degli Studi di Palermo, Viale delle Scienze Ed. 17, 90128 Palermo, Italy

E-mail: francesco.ferrante@unipa.it

Phone: +39 091 23897979. Fax: +39 091 590015

Abstract

The preferred location and the corresponding energetics of zeolite-embedded single metal atoms and small metal particles are hot topics within active sites optimization and catalysts tuning, even as part of bifunctional materials design. In this context, periodic density functional theory was used to provide insights on the interactions of a platinum atom with the microporous cages of a purely silicious β-zeolite framework (BEA). Cluster growth was subsequently addressed, up to Pt_3@BEA systems, following a one-by-one platinum atom addition; platinum migration between cages was taken into account as well. An unbiased approach was employed, which allowed a wide panorama of structures being considered in addition to a thorough analysis in terms of energetics, cluster geometries and cavity distortions. Calculations revealed that the optimal interaction geometry for a single platinum atom is realized where two strong Pt−O bonds in almost linear arrangement can form, regardless of the cavity involved. This can cause distortions or even breaking of the zeolite structure, a factor which however is not decisive in determining the energetics of systems with two and three platinum atoms. Platinum migration is associated with energy barriers ranging from

100 to 200 kJ mol^{-1}, depending on the cages. Up to the dimensions considered here, preference for clustering is observed, being the embedded Pt_3 systems in almost all cases energetically favored with respect to isolated atoms within the BEA framework.

Introduction

Zeolites are crystalline aluminosilicates successfully used as heterogeneous catalysts in many acid-catalyzed reactions, due to their well determined topology and microporous structure, together with the associated adsorption and shape-selective properties.[1,2] Hydroisomerization and hydrocracking of paraffines, alkylation, alkoxylation and selective reduction of nitrogen oxides provide some examples of processes exploiting zeolites Brønsted acid strength. This is associated with the silicon-aluminium framework substitution and the addition of a charge compensating H^+ cation.[3–6] A key factor in these applications is the presence of metallic components, thus forming a bifunctional catalysts,[7] that exploit hydrogenation/dehydrogenation activity of a noble metal such as platinum or palladium. As an acidic component, β-zeolite (BEA) is one of the most notable and extensively used.[8–12] In BEA structure, silicon and oxygen atoms are linked together to form 3D intersecting 12-membered rings (diameter of 6-7 Å along the [010] and [100] axes, 5-6 Å along [001]), together with 6, 5 and 4-membered rings. These give raise to smaller pores which are still wide enough to host metal atoms.[13–15] However, in general, the metal can be located not only inside the cavities but also on the outer surface of the crystals, or even supported on an inorganic binder in composite materials.[16–18] Many experimental efforts have been addressed to study the effects of synthesis variables on the metal location and particle dispersion, which in turn affect activity and selectivity of the catalyst.[19–23] In this respect, a prominent role is played also by the defective sites (mostly silanol groups located on mesopores surface) of which BEA is particularly abundant;[24,25] synthetic strategies can be tuned to exploit defective sites in order to enhance the catalytic activities.[26]

The advantages of an atomistic approach on tuning catalysts properties are well es-

tablished.[27–39] In particular, computational chemistry, mostly based on Density Functional Theory (DFT), had an enormous impact on the development of zeolite catalytic materials and processes.[40–46] As a matter of fact, while Hou *et al.*[47] have investigated, by means of periodic DFT calculations, the stabilization of platinum atom and/or clusters inside the cavities of medium size high-silica zeolites (*i.e.* LTA, SOD, CHA, FAU), to the best of our knowledge, a step by step computational approach on platinum clustering inside large pores of aluminosilicates is still missing. In fact, commonly either singly supported platinum atoms or Pt nanoparticles are considered, without giving any idea about their formation yet.[48–50] In this context, the present work aims at providing atomistic level insights on: i) the preferential location of a platinum atom embedded in β-zeolite cages, ii) the energetics related to platinum atoms' migration and iii) the cluster growth process up to a Pt_3 seed. The investigation employs a one-by-one atom addition approach driven by an unbiased algorithm, described in the next section. Thus, a wide panorama of structures being considered, the analysis is performed on energetics, cluster geometries and cavity distortions. Migration of a platinum atom between different zeolite cages is also addressed, searching for the related transition state. For the here reported study, a pristine BEA structure was employed, being this the necessary starting point for every wider investigation aiming at the characterization of the growth energetics of metal particles in β-zeolite models, which include, *e.g.*, aluminum substitution in different ratios and the presence of various kinds of defects.

Models and Methods

The structural model used for periodic DFT calculations is the β-zeolite unit cell (a = 12.631 Å, b = 12.631 Å, c = 26.186 Å; $\alpha = \beta = \gamma = 90°$) taken from the crystallographic information file provided by the International Zeolite Association (IZA) website.[13] The model structure, see Figure 1, is reported in the IZA atlas as a mixture of α and β BEA polymorphs, most properly labeled as *BEA. After geometry optimization of the silicate structure, a

comprehensive mapping of the embedding sites was performed, with the systematic approach described below, aimed at locating the preferred position for single platinum atoms. Due to the great variety of topological sites characterizing the β-zeolite, an unbiased approach is desirable to fix the starting coordinates of the platinum atoms within the structure. Only by this leading scenario, after geometry optimization of the embedded platinum fragments, it is conceivable to obtain minima suitable to characterize the potential energy surface originating by the different starting configurations. Therefore, the following procedure was implemented. A 3–D grid of points with predefined thickness was created to map BEA unit cell, resulting in 10 points along a and b crystallographic axes (from the 0.00 to the 12.43 coordinate, in Å) and 20 points along c (from 0.00 to 26.21 Å). Each of the 2000 grid points represents a possible set of *xyz* coordinates of an embedded platinum atom. Cases in which the added Pt atom resulted too close to the silicon and/or oxygen atoms of the zeolite framework were excluded based on the van der Waals radii. In particular, the minimum Pt−O (or Pt−Si) distance threshold of 1.8 Å was chosen. In order to discard those geometries showing weak platinum-zeolite interactions, it was fixed, as a further constraint, that the distance between Pt and the nearest framework center should not exceed 3.0 Å. This way 683 cases out of thousands were selected. Single point calculations were performed on the latter and relative energies were used to sort the structures in order of stability. Noticeably, many of them showed almost the same energy, which was ascertained to correspond to similar, if not identical, structures. A relative energy threshold (first sieve) allowed us to single out the most promising 14 cases among the 683. These were subjected to ensuing geometry optimization procedure, which let some structure to collapse to the same geometry minimum (second sieve) and left only 8 Pt-zeolite structures. Following this, another energetic filter (third sieve), ruled by visual inspection, allowed us to select new geometries where to add a second platinum atom. Starting from the creation of a grid of points inside the unit cell, the procedure was repeated on each of these selected geometries to find the best arrangments for two platinum atoms inside the zeolite cages, and repeated once again for the Pt_3@BEA

case. For systems with two or three Pt atoms, minimum and maximum Pt−X (X=Si, O, Pt) distances have also been set. That is, the coordinates of the new atom were accepted if the distance with respect to the platinum atom(s) already present was within the range 2.4-2.8 Å, the thresholds with silicon and oxygen being the same as before. Moreover, the grid step was adjusted, to locate a greater number of geometries in proximity of the already adsorbed Pt center(s). The flowchart of this procedure, aimed at including the largest number of significant structures, is illustrated in Scheme 1. The information related to the different steps of the algorithm for the three Pt_n systems are reported in Table 1. It must be stressed that the criteria adopted for the sieves aimed at reducing the number of possible structures to investigate by isolating the most significant cases. Due to the topological heterogeneity of the analyzed systems, the energetic threshold values were varied, being lower when the number of structures to be selected was greater. In any case, in the course of the analysis, structures were also included, irrespective of their relative energetic stability, which after an accurate visual inspection showed a heuristic potential to evolve into structures of likely interest, when the number of included platinum atoms changed.

The cluster growth was evaluated calculating the ΔE for the following processes:

$$2\,\mathrm{Pt@BEA} \longrightarrow \mathrm{Pt_2@BEA} + \mathrm{BEA} \tag{1}$$

$$3\,\mathrm{Pt@BEA} \longrightarrow \mathrm{Pt_3@BEA} + 2\,\mathrm{BEA} \tag{2}$$

$$\mathrm{Pt_2@BEA} + \mathrm{Pt@BEA} \longrightarrow \mathrm{Pt_3@BEA} + \mathrm{BEA} \tag{3}$$

where the reactants are the same zeolite fragments in which either two or three platinum atoms, or a single atom with a diatomic cluster, were adsorbed but did not interact with each other. The products instead represent a zeolite in which a platinum cluster is formed. A negative value of the concurrent energy differences means that the product cluster formation inside the zeolite is favored.

In order to investigate the distortions of the zeolite cavities produced by the embedding of platinum atoms, a point R, whose coordinates matched those of the first embedded plat-

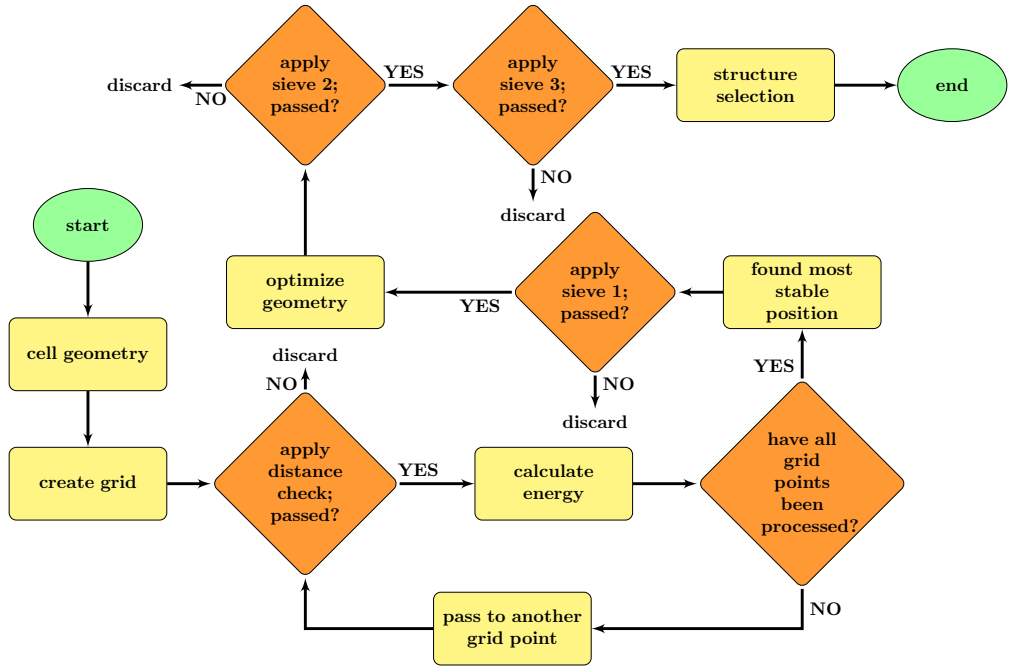

Scheme 1: Flowchart of the algorithm employed to locate the preferential position of a single platinum atom and to study the cluster formation. At the beginning of the procedure, the starting geometry is the optimized silicate framework; selected geometries are then used as input for the second and third platinum atom addition.

inum atom, was chosen and around this the zeolite nuclei distribution was explored. In these structures, all O−R and Si−R distances (corresponding to the O−Pt and Si−Pt distances in the Pt-zeolite system) were computed and then sorted in increasing order. After choosing an exploration radius around R, all the nuclei at a distance greater than this radius were discarded, thus narrowing the analysis focus closer to R. Considering the cell parameters of the employed model, we chose a value of 6.2 Å for the exploration radius, thus avoiding spurious effects caused by periodic boundary conditions, while still encompassing an appropriately large number of zeolite nuclei. For each oxygen and silicon center included in the exploration radius of single couples of pristine and platinum-emebedded structures, two displacements are computed. The first is the absolute displacement of nucleus A, $\Delta_a^A \equiv |\mathbf{R}_\mathrm{p}^A - \mathbf{R}_\mathrm{e}^A|$, attributable to the platinum presence, where $\mathbf{R}_\mathrm{p}^A$ are the coordinates of A in the pristine zeolite, and $\mathbf{R}_\mathrm{e}^A$ those in the embedded zeolite. The second, conversely, is the radial displacement of A with respect to the central point R, $\Delta_r^A \equiv |\mathbf{R}_\mathrm{e}^A - \mathbf{R}| - |\mathbf{R}_\mathrm{p}^A - \mathbf{R}|$.

Computational Details

All calculations were performed within the density functional theory framework (DFT) by using the SIESTA approach as implemented in the code bearing the same name.[51] The PBE exchange-correlation functional in the spin-polarized form was chosen,[52] along with a double-ζ quality numerical basis set. Sampling of reciprocal space was performed using a 2×2×2 Monkhorst-Pack grid and a value of 450 Ry for the mesh cutoff. Preliminary calculations performed in selected cases allowed to conclude that a larger Monkhorst-Pack grid affected the energy of the investigated systems in a negligible way.

The search for transition states associated with the Pt atom migration was performed by means of the Empathes code,[53] which implements the Nudged Elastic Band method (NEB) and is interfaced with the SIESTA program. Every NEB calculation used 8 images, generated by the image dependent pair potential approach and connected each other by dynamic springs. The FIRE algorithm was employed to optimize the elastic band, with a convergence threshold of (5×10^{-3} E_h/Å) on the norm of NEB total forces.

Results and Discussion

Single Pt atom embedded in BEA cages

As shown by Table 1, 8 different structures have been identified for the adsorption of a single platinum atom within the BEA framework. In these, the metal atom is inside a unique zeolite cavity. The energy differences characterizing the various structures can be attributed to the occurrence of different local topologies. It is noteworthy that, even if spin polarized calculations were performed, the results obtained for all the investigated systems always indicate a singlet multiplicity state. As a matter of fact, this is in agreement with other evidences of spin state lowering that takes place in supported system when a platinum atom is interacting with the zeolite framework with respect to unsupported ones.[47] Figure 2

shows a local view of the eigth optimized geometries. To emphasize the visualization of the rings and cavities involved, it was decided to not show the whole unit cell. In each case, a portion of the zeolite framework close to the Pt atom was conversely selected for the image representation, obtained by repeating the unit cell in space when needed. In accordance with the tiling arrangement accepted by IZA,[13] the optimized structures can be divided into the following five groups:

- t-bet cavity, in which the Pt atom interacts with 5-membered rings (5T);
- t-mtw cavity, with the Pt atom located in-between two 6-membered rings;
- t-bea-1* cavity, where the Pt atom protrudes towards the main channel and interacts with 5T or 4T rings;
- t-umx* cavity, in which the Pt atom interacts with a 6T ring in a main channel;
- t-bea-2* cavity, where the Pt atom located in the main channel is near but not inside the t-bet cavity.

Among the final Pt@BEA systems here investigated, four cases can be assigned to the t-bea-1* cavity and these, in order to be distinguished, are labeled with additional letters "a-d". In Figure 2, significant structural parameters are shown above the corresponding structures. In details they are the bond distances between platinum and the two nearest oxygen atoms, and the related O−Pt−O bond angle. Finally, relative energies are also indicated. These were calculated as the difference between the energy corresponding to the structure of the involved system and that of the most stable one, taken as reference. Accordingly, an order of stability among the structures could be extrapolated. Those containing the t-bet smallest cavities resulted preferred, followed by those showing 6T ring pore. Systems in which platinum is located within the main channel are up to 80-110 kJ mol^{-1} higher in energy with respect to the most stable Pt@t-bet species.

Analyzing things more in depth, it can be inferred that this trend is not strictly dependent on the channel sizes, but rather on local interactions involving different zeolite surface fragments and metal atoms. In details, in the most stable configurations, platinum is found to form strong bonds with a couple of oxygen atoms (2.09-2.12 Å) and, more importantly, an almost straight O–Pt–O bond angle. In particular, it seems that, regardless of the involved cavity size, optimized structures are more stable when the O–Pt–O angle is close to 180°. In this context it is possible to frame the energetics of Pt@t-bea-1*(a) and Pt@t-bea-1*(b) species, showing O–Pt–O angles of 178.6 and 175.2°, respectively. In these the platinum atom embedded in the main channel is in fact stabilized by an energy that is close to that observed for the same metal atom when allocated in a smaller cavity. It can be conversely observed that the four t-bea-1* fragments hosting the platinum atom in the same cavity show energies that vary in a significant way, and stronger interations invariably occur when the O–Pt–O bond angle is almost linear. Finally, it is important to note that in the case of Pt@t-bea-1*(a) and Pt@t-bea-1*(b) species, the formation of this particular bond angle was driven by the displacement of an oxygen atom from the silicon to which it was bonded, resulting in a visible alteration of the framework regularity, which will be further discussed later on.

Pt migration

In the hypothesis that a given metal atom approaches the smaller cages of a zeolite from its main channels, platinum migration from the latter to the Pt@t-bet cavity was modeled according to this mechanism. The metal shift between the two smaller cavities was also studied. In the first process, the Pt@t-bea-1*(b) species was chosen as the starting arrangement to represent a system bearing a platinum atom in the main channel. From this, Pt atom shift took place in two steps, going through an intermediate, which resulted to be 20.5 kJ mol^{-1} more stable than the corresponding system and 13.1 kJ mol^{-1} higher in energy if compared with the final one (see Figure S1). The two energy barriers, namely those from

the reactant to the intermediate and from this one to the Pt@t-bet product resulted 102.6 and 127.6 kJ mol^{-1}, respectively.

In the second process the platinum atom migrates in a single step (an high energy ephemeral intermediate is actually in the path), crossing the wall that separates the two cavities; the associated energy barrier was equal to 203.4 kJ mol^{-1}. It is interesting to note that, over the minimum energy path found by the NEB calculation (Figure S2), the platinum atom rotates by pivoting on an oxygen bridging the two cavities. As a consequence, a breakage in the zeolite structure is observed, while the O−Si bond distances get back to the usual values in the product. The occurrence of structures that show the breaking of the zeolite framework deserves further discussion. In fact, this has already been discussed in the literature for zeolites with 6-membered rings,[47] where that situation represented the most stable configuration for an embedded platinum atom. In our case it is interesting to note how geometries were found in which the breaking occured in the proximity of a 5T ring. This kind of structure, however, features an energy sensibly higher than that of the stablest structures found with the systematic search algorithm employed in the present work (see Scheme 1).

Pt_2 and Pt_3 clusters inside BEA framework

Starting from the four most stable geometries with one adsorbed platinum atom, 12 cases of Pt_2@BEA systems have been identified (see Table 1) and five were selected after having applied the third sieve. All systems, whose optimized geometries are reported in Figure 3, resulted to be in a singlet multiplicity state. In the most stable of them, the second platinum atom i) is placed at about 2.5 Å from the first, ii) slightly protrudes into the main zeolite channel and iii) attracts one oxygen atom forming an almost straight bond angle. Two pretty similar cases follow. In this, once again, the first platinum atom is located in the t-mtw cavity and the second, positioned in the main t-bea-1* channel, attracts one oxygen atom towards itself to form an almost linear bond angle. In a *ca.* 50 kJ mol^{-1} less stable

arrangement, the first Pt atom is located in the smaller t-bet cavity, while the second, at 2.87 Å from the first, protrudes into the main channel and causes the rupture of the zeolite framework with the formation of a 176.7° O−Pt−O bond angle. Notably, two of these platinum-oxygen interactions, which seemingly rule the energetics of Pt@BEA adducts, are present. Since the analysis performed on the framework (see Section "Cavity distortions") showed minor distortions, the lower stability of this system can be interpreted in terms of the Pt−Pt distance. In fact, the interaction between the two metal atoms is rather weak, being the bond distance sensibly higher than the optimal value of 2.34 Å, obtained for the isolated Pt_2 dimer in the triplet state, at the same calculation level of theory. Finally, two platinum atoms at 2.78 Å from each other are located in the t-bea-1* channel and share an oxygen atom to form bond angles that strongly deviates from the linearity (151.5° and 169.8°), presumably leading for this reason to the less stable among the considered Pt_2@BEA systems, being its relative energy 61.9 kJ mol^{-1}.

The tendency of platinum to cluster was evaluated for the various cases, and it was found a clustering behaviour that allows to further justify the particular stability of the Pt_2@t-mtw structures, where the platinum atoms are more intimately bonded. Thus, the Pt−Pt distance plays a significant role to understand the energetics of Pt_2@BEA systems, together with the O−Pt−O interactions and framework distortions.

An analogous analysis was performed for the addition of the third platinum atom. According to the proposed systematic approach, 14 Pt_3@BEA structures were identified and grouped in 5 sets originating by the Pt_2@BEA system (see Table 1). In the following, however, only minima within 30 kJ mol^{-1} of relative energy are taken into account for each cavity group, for a total of 8 cases. The optimized structures, all in the singlet multiplicity state, are reported in Figure 4, together with significant structural parameters of the three metal atoms. In the most stable case two platinum atoms are located inside the t-mtw cavity, with the third Pt that protrudes into the main channel, forming an isosceles triangle characterized by Pt−Pt bond distances of 2.56, 2.57 and 2.72 Å. Only one platinum atom, the second in

order of addition to the zeolite structure, features the typical O−Pt−O interaction. In a nearly 35 kJ mol^{-1} less stable structure, the Pt_3 cluster assumes the shape of an isosceles triangle, reversed with respect to the previous case, that is with a single Pt inside the t-mtw cavity and the other two in the main channel. The second platinum atom evenly interacts with 3 oxygen atoms and there is a rupture of the zeolitic framework regularity due to the formation of the linear O−Pt−O configuration, further discussed in the next section. With the third structure, named Pt_3@t-bea-1*(a), the relative energy rises to 118.2 kJ mol^{-1} and the cluster assumes the shape of a scalene triangle at the intersection between the two main 12T channels of BEA. Two platinum atoms share an oxygen within the favorable O−Pt−O interacting mode, and consequently framework distortions are present as for Pt_2@t-bea-1* system. The fourth system, characterized by a relative energy of 140.5 kJ mol^{-1}, features an almost linear arrangement of the three platinum atoms (angle 171.4°) with distances equal to 2.52 and 2.56 Å. Only the second Pt atom interacts with two oxygens in the linear O−Pt−O fragment, being the framework just slightly perturbed. At almost equal energy (144.8 kJ mol^{-1}) a new structure similar to the other Pt_3@t-bea-1* follows in which, however, the scalene triangle formed by the Pt_3 cluster at the intersection between the channels has fewer interactions with the zeolite walls: this is especially true for the third platinum atom, which finds the closest oxygen 3.66 Å apart. Only the first Pt shows the preferential interaction with two oxygens and due to this a t-bet cavity is broken, as happened for the same site with one and two platinum atoms. The last three systems, belonging to the t-bet group, are characterized by the fact that the Pt_3 cluster assumes a bent shape with angles of 85.1°, 86.4°and 88.6°, going towards the least stable case, which has a relative energy of 193.1 kJ mol^{-1}. In these systems, irrespective of the involved energy, two platinum atoms interact with two oxygen atoms, being the connected cavity broken, while the third Pt only sees a single O atom nearby.

Overall, it is evident the sensible difference in energy among the 8 selected systems, where the first two differ by 35.2 kJ mol^{-1} while the less stable structure is nearly 190 kJ mol^{-1}

higher in energy than the Pt_3@t-mtw(c) reference. These findings can be rationalized in terms of the embedded cluster geometry compared to that of the *in-vacuo* Pt_3 structure, investigated at the same computational level. The latter indeed appears to be an equilateral triangle in singlet multiplicity state, with Pt−Pt bond distances of 2.48 Å. It can be argued, by comparing the more and less stable cases, that the system is more stable as the embedded Pt_3 cluster gets closer to this ideal configuration. The second factor determining the stability of the studied systems is the possibility of interactions with the zeolite walls; in these terms we can in fact interpret the energetic order found between the two Pt_3@t-bea-1* cases. Interestingly, Pt_3@t-mtw(a), where a linear arrangement occurs, has an energy in-between the two Pt_3@t-bea-1* systems. It evidently represents a peculiar zeolitic fragment suitable to accommodate, without the occurrence of large framework distortions, the three platinum atoms, characterized by Pt−Pt bond distances similar to those of both the more stable Pt_3@BEA system and the *in-vacuo* triangular platinum cluster.

Cavity distortions

Figures 5 to 7 display the graphs obtained by performing a framework distortion analysis focused on the oxygen atoms, following the approach outlined in the "Models and Methods" section, for all the Pt_n@BEA systems. Accordingly, in a given graph, the values in the abscissa represent the distance between the reference point R and the oxygen atoms in the pristine BEA cell, while in the ordinate are reported the modules of both the absolute (Δ_a^{O}) and radial (Δ_r^{O}) displacements from that distance. The corresponding graphs that refer to the silicon atoms are reported in Figures S3-S5 of SI. Incidentally, for Pt@BEA structures only the cases corresponding to cavities for which the equivalent systems with two and three platinum atoms are present were taken into account; the t-bea-1*(b) species of Figure 2 was, for example, not considered. The graph relating to the t-bet system in Figure 5 shows minimal distortions; in fact, the two most intense peaks consist of displacements by approximately 0.3 and 0.2 Å, while all the silicon positions in the framework remains almost

unchanged (see Figure S3). These data allow one to interpret the particular stability of the t-bet cage structure: the O−Pt−O interaction occurs naturally into a frame that is quite already suitable, in terms of volume and zeolite framework topology, to effectively host one platinum atom. Rising in relative energy, the graph of the t-mtw system shows, among all, 5 oxygen peaks between 2.10 and 2.80 Å, mostly of the radial kind, whose absolute displacements range from 0.4 to 0.8 Å. They correspond to five of the t-mtw cavity oxygen atoms closer to the reference point R. Therefore, these oxygen centers undergo sensible modifications when Pt is inserted, while once again the Si atoms mostly maintain their positions, since the oxygen atom rotates around the Si−O−Si axis. The last graph of Figure 5 shows several oxygen peaks with magnitude greater than 0.5 Å: at 1.45 Å, 2.40 Å, 2.46 Å and then again at 3.79 Å. Also two silicon atoms have undergone displacements of *ca.* 0.4 Å. The corresponding distortions showed different Δ characters, as proved by the peaks at 2.18 and 2.32 Å in Figure S3. Analyzing the structure in more details, it can be observed that the latter are indeed coupled with the first two oxygen signals discussed above, jointly corresponding to a situation in which the framework is broken. In fact, the silicon atoms move away from each other, each bringing an oxygen atom with itself. As a consequence, there is a Si−O distance of 2.66 Å (whereas in the pristine zeolite framework it is 1.66 Å).

Moving to systems with two zeolite-embedded platinum atoms, Figure 6 shows the Δ_a^{O} and Δ_r^{O} characteristics of the two platinum atoms systems. The first three panels, corresponding to the most stable t-mtw structures, exhibit several intense (up to 1.1 Å of absolute displacement) and closely spaced peaks in the range between 2.17 and 3.57 Å. This finding lets to infer that for the Pt_2@BEA systems, the zeolite distortions are not predominant in destabilizing the supported structures with respect to the original BEA units. The box relating to the Pt_2@t-bet species is characterized by very slight distortions compared to the others, despite the presence of a peak for oxygen at *ca.* 3.10 Å, with a distortion value close to 1.0 Å, and two peaks for silicon at distances of 2.76 and 3.95 Å, both showing a distortion value equal to 0.4 Å (see Figure S4), that were negligible in the graph of the

Pt@t-bet system. They correspond to a break of the zeolite framework in which the Si atom, showing larger radial displacements, moves away, jointly with the oxygen atom, from the other silicon so that the latter is found at a distance of 2.83 Å (against 1.66 Å of the original structure). The driving force of this break can be identified in the oxygen attraction exerted by the platinum atom to form an almost linear arrangement. Finally, for the less stable Pt_2@t-bea-1* structure the same peaks of Si and O that characterized the cavity with a single embedded platinum atom are present, only subjected both to subtle variations in magnitude and to the already discussed framework modifications. It is interesting to point out that the first oxygen peak, located at 1.45 Å and showing a distortion value equal to 1.3 Å, is now associated with one O−Pt−O interaction mode between the oxygen and both the two metal atoms, as discussed in the previous section. Furthermore, this peak and the one centered at 2.46 Å have radial displacements in the average, but they reach the maximum values of the absolute displacement among all the systems.

Figure 7 reports the distortion behaviors taking place in the different BEA cavities related to systems with three platinum atoms embedded in the zeolite framework. The most stable Pt_3@t-mtw(c) case unveils the two highest peaks (1.18 and 1.06 Å) at 2.73 and 3.57 Å from the center taken as reference, thus being very similar to the behavior of the corresponding site with two platinum atoms, in fact only the second peak became slightly more intense. The next panel shows the same peaks in the range 2.17–3.57 Å that were already observed for the Pt_2@t-mtw structures, with little changes in the signal behaviors. The one at 3.22 Å couples with the silicon peak at 2.94 Å of 1.08 Å of absolute displacement (which conversely was negligible in the Si graph of the supported Pt_2 structure) in a break of the zeolitic framework where the two atom move apart to a final Si-O distance of 3.30 Å. An off-scale oxygen peak is also observed, corresponding to an O atom that moved, significantly, in order to bond with two other silicon atoms different to those present in the initial couple. Its position is now actually occupied by the added third platinum atom. The behavoir of t-bea-1*(a) has not undergone substantial changes passing from the system involving two to that involving three

embedded platinum atoms, neither for oxygen nor for silicon displacement. The same result observing the the subsequent panel and the, there represented, Pt_2@t-mtw(a) system. The Pt_3@t-bea-1*(b) species presents a framework break produced by the first Pt atom already added to the zeolite. However, the graph shows less intense peaks with respect to both its parent structures having one and two platinum atoms. Pt_3@t-bea-1*(a) is less stable than the related (b) one, due to fewer interactions occurring between the cluster and the zeolite walls. The values reported in the panels regarding the Pt_3@t-bet geometry group are very similar to each other. If compared to the equivalent structures characterized by the presence of two platinum atoms, the O and Si peaks related to the rupture of the framework are once again systematically observed, being those of silicon at slightly higher intensity (0.50-0.60 Å against the previous values of 0.40 Å, see Figures 7 and S5). Furthermore, other peaks of oxygen atoms reaching values of about 1.0 Å are also present, with a characteristic prevalence of an angular component of the displacement, as can be deduced by the large difference between Δ_a^{O} and Δ_r^{O}.

Energetics of the clustering process

The tendecy to clustering was evaluated inside all the considered cavities by calculating the ΔE values according to processes (1)-(3). The results are collected in Table 2. Besides, Figure 8 shows the relative energies concerning sets of systems characterized by the presence of embedded Pt cluster having a different number (1-3) of atoms inside the cavities. As can be noticed from the negative values in the first column, Pt_2 clusters are favored over two isolated Pt atoms, and this is true regardless the kind of cavity. The greatest tendency towards growth however occurs in the cases where the t-mtw cavity is involved. This is the second in order of stability as regards the location of a single platinum atom, but is actually energetically the preferred over the others for the Pt_2@BEA systems. The structures involved in the different systems easily explain these findings. In fact, as previously highlighted, the t-bet cavity is already suitable for hosting one platinum atom, while the t-mtw cavity

undergoes distortions of the framework. However, in the latter, two metal atoms exhibit a smaller bond distance hence higher cluster-like features.

The values reported in the second column shows that Pt_3@BEA systems are favored over three isolated atoms, except for the t-bet sites. Growth in this cavity is indeed thermodynamically unfavorable. This is not surprising given that in this case a comparison is performed between the worst condition for clustering within the Pt_3 group (see Figure 8) with the best energetic condition that is possible to find for a single Pt embedded in the zeolite. From the structural point of view, the t-bet cavity is too small to accommodate the three platinum atoms; in fact already the second Pt added in this cavity protrudes towards the main channel, so that the cluster is characterized by little interactions with the zeolite walls. In the case of the other two types of cavities, on the other hand, the presence of a Pt_3 particle is strongly favored, with ΔE values ranging from about 115 to 240 kJ mol^{-1}.

The third column of Table 2 shows the difference between the energy of an embedded Pt_3 cluster in a given cavity and the energy of both one metal dimer and one metal atom placed in two distinct cavities of the same type. The positive value of +18.1 kJ mol^{-1} characterizing the t-mtw(a) cavity, see Table 2, stands out, as an example, from this kind of data adjustment, which leads to an internal comparison of the three possible structures in the t-mtw group. If the preferred system for two platinum atoms is the first, the addition of a further Pt atom leads to a not particularly stable situation, due to the lack of significant interactions between the metal triangle-shaped cluster and the zeolite framework. Thus the growth process to Pt_3 most likely follows the c-type structure formation.

Needless to say, clustering could be further investigated, even until complete saturation of the main zeolite channel is reached. However, this is clearly outside the scope of the present work, since the studied systems are intended to be used as catalysts. Thus, on the contrary, a minimum size is desirable provided that the corresponding minimum size cluster is effective to have catalytic activity hence, as prerequisite, is available to interact with substrates in the main zeolite channel.

Conclusions

An approach within the DFT framework was employed to identify preferential location of platinum atoms inside a β-zeolite model and to study the growth of a minimal cluster. Pt atoms migration through cages was also addressed, by means of a transition state search following the NEB approach.

A comparative structural analysis involving different cavities and platinum atom numbers showed that the optimal geometry involving a single platinum atom takes place when the formation of a O−Pt−O unit in an almost linear arrangement occurs. This seems to be the driving force that mainly determine the local structure properties of the metal-functionalized BEA and may cause breaking of the zeolite structure even when only one platinum atom is included in a cage. Energetic preference for clustering was observed against the occurring of multiple distinct interactions between zeolite sites and metal centers, leading to slightly different cluster geometries. With respect to this, the Pt−Pt distance is actually a sensible factor in orienting the energetics of the Pt_2@BEA species while the cluster geometry become very significant in the case of the Pt_3@BEA species, where the closer the shape of the cluster is to that of an equilateral triangle, the more stable the corresponding fragment results.

Platinum migration characterized by the crossing of the wall of different cavities may occur with relatively low energy barriers, although occasionally, due to the local topology, the same process could be hindered by prohibitive energy values.

Since zeolite systems with metal atoms protruding towards the main zeolite channel, where reactions are likely to occur, have potential catalytic activity, future developments will be addressed to simulate, on Pt-embedded zeolites, catalytic reactions of interest in the fuel industry, such as paraffines hydrogenation/dehydrogenation, as part of hydroisomerization or cracking processes.

Supporting Information Available

Diagrams representing minimum energy paths for Pt migration between the zeolite cages; graphs for silicon atom displacement analysis; optimized geometries of the most stable Pt_n@BEA systems in xyz format.

References

(1) Ennaert, T.; Van Aelst, J.; Dijkmans, J.; De Clercq, R.; Schutyser, W.; Dusselier, M.; Verboekend, D.; Sels, B. F. Potential and Challenges of Zeolite Chemistry in the Catalytic Conversion of Biomass. *Chem. Soc. Rev.* **2016**, *45*, 584–611.

(2) Mäki-Arvela, P.; Kaka Khel, T. A.; Azkaar, M.; Engblom, S.; Murzin, D. Yu. Catalytic Hydroisomerization of Long-Chain Hydrocarbons for the Production of Fuels. *Catalysts* **2018**, *8*, 534.

(3) Sun, Y.; Han, S. Mechanistic Investigation of Methanol to Propene Conversion Catalyzed by H-Beta Zeolite: A Two-Layer ONIOM Study. *J. Mol. Model.* **2013**, *19*, 5407–5422.

(4) Boroń, P.; Rutkowska, M.; Gil, B.; Marszalek, B.; Chmielarz, L.; Dzwigaj, S. Experimental Evidence of the Mechanism of Selective Catalytic Reduction of NO with NH_3 over Fe-Containing BEA Zeolites. *ChemSusChem* **2019**, *12*, 692–705.

(5) Gramigni, F.; Selleri, T.; Nova, I.; Tronconi, E. Catalyst Systems for Selective Catalytic Reduction + NO_x Trapping: from Fundamental Understanding of the Standard SCR Reaction to Practical Applications for Lean Exhaust After-Treatment. *React. Chem. Eng.* **2019**, *4*, 1165–1178.

(6) Berger, F.; Rybicki, M.; Sauer, J. Adsorption and Cracking of Propane by Zeolites of Different Pore Size. *J. Catal.* **2021**, *395*, 117–128.

(7) Wang, H.; Wang, L.; Xiao, F.-S. Metal@Zeolite Hybrid Materials for Catalysis. *ACS Cent. Sci.* **2020**, *6*, 1685–1697.

(8) Nie, X.; Janik, M. J.; Guo, X.; Liu, X.; Song, C. Reaction Mechanism of tert-Butylation of Phenol with tert-Butyl Alcohol over H-β Zeolite: An ONIOM Study. *Catal. Today* **2011**, *165*, 120–128.

(9) Gomes, L. C.; de Oliveira Rosas, D.; Chistone, R. C.; Zotin, F. M. Z.; de Araujo, L. R. R.; Zotin, J. L. Hydroisomerization of n-Hexadecane using Pt/Alumina-Beta Zeolite Catalysts for Producing Renewable Diesel with Low Pour Point. *Fuel* **2017**, *209*, 521–528.

(10) Kaka Khel, T.; Päivi, M. A.; Azkaar, M.; Vajglová, Z.; Aho, A.; Hemming, J.; Peurla, M.; Eränen, K.; Kumar, N.; Murzin, D. Yu. Hexadecane Hydrocracking for Production of Jet Fuels from Renewable Diesel over Proton and Metal Modified H-Beta Zeolites. *Mol. Catal.* **2019**, *476*, 110515.

(11) Guo, Y.; Du, X.; Liu, L.; Dong, Y.; Lei, Z. Reaction Mechanism of Benzene Alkylation with Propylene Catalyzed by HZSM-5 Zeolite and H-Beta Zeolite. *Mater. Today Commun.* **2021**, *26*, 101757.

(12) Laluc, M.; Barakov, R.; Mäki-Arvela, P.; Shcherban, N.; Murzin, D. Yu. Catalytic Activity of Hierarchical Beta Zeolites in the Prins Cyclization of (−)-Isopulegol with Acetone. *Appl. Catal. A: Gen.* **2021**, *618*, 118131.

(13) Database of Zeolite Structures @ http://www.iza-structure.org/databases/. `http://www.iza-structure.org/databases/`, (accessed July 17, 2020).

(14) Vjunov, A.; Fulton, J. L.; Huthwelker, T.; Pin, S.; Mei, D.; Schenter, G. K.; Govind, N.; Camaioni, D. M.; Hu, J. Z.; Lercher, J. A. Quantitatively Probing the Al Distribution in Zeolites. *J. Am. Chem. Soc.* **2014**, *136*, 8296–8306.

(15) Li, S.; Zhao, Z.; Zhao, R.; Zhou, D.; Zhang, W. Aluminum Location and Acid Strength in an Aluminum-Rich Beta Zeolite Catalyst: A Combined Density Functional Theory and Solid-State NMR Study. *ChemCatChem* **2017**, *9*, 1494–1502.

(16) Batalha, N.; Pinard, L.; Pouilloux, Y.; Guisnet, M. Bifunctional Hydrogenating/Acid Catalysis: Quantification of the Intimacy Criterion. *Catal. Lett.* **2013**, *143*, 587–591.

(17) Gutierrez-Acebo, E.; Leroux, C.; Chizallet, C.; Schuurman, Y.; Bouchy, C. Metal/Acid Bifunctional Catalysis and Intimacy Criterion for Ethylcyclohexane Hydroconversion: When Proximity Does Not Matter. *ACS Catal.* **2018**, *8*, 6035–6046.

(18) Mendes, P. S. F.; Silva, J. M.; Ribeiro, M. F.; Daudin, A.; Bouchy, C. From Powder to Extrudate Zeolite-Based Bifunctional Hydroisomerization Catalysts: on Preserving Zeolite Integrity and Optimizing Pt Location. *J. Ind. Eng. Chem.* **2018**, *62*, 72–83.

(19) Wang, Y.; Tao, Z.; Wu, B.; Xu, J.; Huo, C.; Li, K.; Chen, H.; Yang, Y.; Li, Y. Effect of Metal Precursors on the Performance of Pt/ZSM-22 Catalysts for n-Hexadecane Hydroisomerization. *J. Catal.* **2015**, *322*, 1–13.

(20) Liu, L.; Lopez-Haro, M.; Lopes, C. W.; Li, C.; Concepcion, P.; Simonelli, L.; Calvino, J. J.; Corma, A. Regioselective Generation and Reactivity Control of Subnanometric Platinum Clusters in Zeolites for High-Temperature Catalysis. *Nat. Mater.* **2019**, *18*, 866–873.

(21) Liu, Y.; Li, Z.; Yu, Q.; Chen, Y.; Chai, Z.; Zhao, G.; Liu, S.; Cheong, W.; Pan, Y.; Zhang, Q. et al. A General Strategy for Fabricating Isolated Single Metal Atomic Site Catalysts in Y Zeolite. *J. Am. Chem. Soc.* **2019**, *141*, 9305–9311.

(22) Tian, Y.; Duan, H.; Zhang, B.; Gong, S.; Lu, Z.; Dai, L.; Qiao, C.; Liu, G.; Zhao, Y. Template Guiding for the Encapsulation of Uniformly Subnanometric Platinum Clusters in Beta-Zeolites Enabling High Catalytic Activity and Stability. *Angew. Chem. Int. Ed. Eng.* **2021**, *60*, 21713–21717.

(23) Vajglová, Z.; Kumar, N.; Peurla, M.; Hupa, L.; Semikin, K.; Sladkovskiy, D. A.; Murzin, D. Yu. Effect of the Preparation of Pt-Modified Zeolite Beta-Bentonite Extrudates on Their Catalytic Behavior in n-Hexane Hydroisomerization. *Ind. Eng. Chem. Res.* **2019**, *58*, 10875–10885.

(24) Wright, P. A.; Zhou, W.; Pérez-Pariente, J.; Arranz, M. Direct Observation of Growth Defects in Zeolite Beta. *J. Am. Chem. Soc.* **2005**, *127*, 494–495.

(25) Medeiros-Costa, I. C.; Dib, E.; Nesterenko, N.; Dath, J.-P.; Gilson, J.-P.; Mintova, S. Silanol Defect Engineering and Healing in Zeolites: Opportunities to Fine-Tune their Properties and Performances. *Chem. Soc. Rev.* **2021**, *50*, 11156–11179.

(26) Kokuryo, S.; Miyake, K.; Uchida, Y.; Mizusawa, A.; Kubo, T.; Nishiyama, N. Defect Engineering to Boost Catalytic Activity of Beta Zeolite on Low-Density Polyethylene Cracking. *Mater. Today Sustain.* **2022**, *17*, 100098.

(27) Gambo, Y.; Adamu, S.; Abdulrasheed, A. A.; Lucky, R. A.; Ba-Shammakh, M. S.; Hossain, M. M. Catalyst Design and Tuning for Oxidative Dehydrogenation of Propane - A Review. *Appl. Catal. A: Gen.* **2021**, *609*, 117914.

(28) Vorontsov, A. V.; Valdés, H.; Smirniotis, P. G. Design of Active Sites in Zeolite Catalysts Using Modern Semiempirical Methods: The Case of Mordenite. *Comput. Theor. Chem.* **2019**, *1166*, 112572.

(29) Prestianni, A.; Ferrante, F.; Sulman, E. M.; Duca, D. Density Functional Theory Investigation on the Nucleation and Growth of Small Palladium Clusters on a Hyper-Cross-Linked Polystyrene Matrix. *J. Phys. Chem. C* **2014**, *118*, 21006–21013.

(30) Ferrante, F.; Prestianni, A.; Duca, D. Computational Investigation of Alkynols and Alkyndiols Hydrogenation on a Palladium Cluster. *J. Phys. Chem. C* **2014**, *118*, 551–558.

(31) Ferrante, F.; Prestianni, A.; Cortese, R.; Schimmenti, R.; Duca, D. Density Functional Theory Investigation on the Nucleation of Homo- and Heteronuclear Metal Clusters on Defective Graphene. *J. Phys. Chem. C* **2016**, *120*, 12022–12031.

(32) Cortese, R.; Schimmenti, R.; Ferrante, F.; Prestianni, A.; Decarolis, D.; Duca, D. Graph-Based Analysis of Ethylene Glycol Decomposition on a Palladium Cluster. *J. Phys. Chem. C* **2017**, *121*, 13606–13616.

(33) Guo, X.; Huang, S. Tuning Nitrogen Reduction Reaction Activity via Controllable Fe Magnetic Moment: A Computational Study of Single Fe Atom Supported on Defective Graphene. *Electrochim. Acta* **2018**, *284*, 392–399.

(34) Cortese, R.; Schimmenti, R.; Prestianni, A.; Duca, D. DFT Calculations on Subnanometric Metal Catalysts: A Short Review on New Supported Materials. *Theor. Chem. Acc.* **2018**, *137*, 59.

(35) Cortese, R.; Campisi, D.; Prestianni, A.; Duca, D. Alkane Dehydrogenation on Defective BN Quasi-Molecular Nanoflakes: DFT Studies. *Mol. Catal.* **2020**, *493*, 110891.

(36) Ferrante, F.; Prestianni, A.; Bertini, M.; Duca, D. H_2 Transformations on Graphene Supported Palladium Cluster: DFT-MD Simulations and NEB Calculations. *Catalysts* **2020**, *10*, 1306.

(37) Gueci, L.; Ferrante, F.; Prestianni, A.; Di Chio, R.; Patti, A. F.; Duca, D.; Arena, F. DFT Insights into the Oxygen-Assisted Selective Oxidation of Benzyl Alcohol on Manganese Dioxide Catalysts. *Inorg. Chim. Acta* **2020**, *511*, 119812.

(38) Gueci, L.; Ferrante, F.; Prestianni, A.; Arena, F.; Duca, D. Benzyl Alcohol to Benzaldehyde Oxidation on MnO_x Clusters: Unraveling Atomistic Features. *Mol. Catal.* **2021**, *513*, 111735.

(39) Arena, F.; Ferrante, F.; Di Chio, R.; Bonura, G.; Frusteri, F.; Frusteri, L.; Prestianni, A.; Morandi, S.; Martra, G.; Duca, D. DFT and Kinetic Evidences of the Preferential CO Oxidation Pattern of Manganese Dioxide Catalysts in Hydrogen Stream (PROX). *Appl. Catal. B: Env.* **2022**, *300*, 120715.

(40) Broclawik, E.; Kozyra, P.; Mitoraj, M.; Radoń, M.; Rejmak, P. Zeolites at the Molecular Level: What Can Be Learned from Molecular Modeling. *Molecules* **2021**, *26*, 1511.

(41) Barone, G.; Li Manni, G.; Prestianni, A.; Duca, D.; Bernas, H.; Murzin, D. Yu. Hydrogenolysis of Hydroxymatairesinol on Y Derived Catalysts: A Computational Study. *J. Mol. Catal. A: Chem.* **2010**, *333*, 136–144.

(42) Ferrante, F.; Rubino, T.; Duca, D. Butene Isomerization and Double-Bond Migration on the H-ZSM-5 Outer Surface: A Density Functional Theory Study. *J. Phys. Chem. C* **2011**, *115*, 14862–14868.

(43) Prestianni, A.; Cortese, R.; Duca, D. Propan-2-ol Dehydration on H-ZSM-5 and H-Y Zeolite: A DFT Study. *React. Kinet. Mech. Catal.* **2013**, *108*, 565–582.

(44) Jones, A. J.; Iglesia, E. The Strength of Brønsted Acid Sites in Microporous Aluminosilicates. *ACS Catal.* **2015**, *5*, 5741–5755.

(45) Klinyod, S.; Boekfa, B.; Pornsatitworakul, S.; Maihom, T.; Jarussophon, N.; Treesukol, P.; Wattanakit, C.; Limtrakul, J. Theoretical and Experimental Study on the 7-Hydroxy-4-Methylcoumarin Synthesis with H-Beta Zeolite. *ChemistrySelect* **2019**, *4*, 10660–10667.

(46) Ren, Q.; Rybicki, M.; Sauer, J. Interaction of C3-C5 Alkenes with Zeolitic Brønsted Sites: π-Complexes, Alkoxides, and Carbenium Ions in H-FER. *J. Phys. Chem. C* **2020**, *124*, 10067–10078.

(47) Hou, D.; Grajciar, L.; Nachtigall, P.; Heard, C. J. Origin of the Unusual Stability of Zeolite-Encapsulated Sub-Nanometer Platinum. *ACS Catal.* **2020**, *10*, 11057–11068.

(48) Xu, D.; Wang, S.; Wu, B.; Huo, C.; Qin, Y.; Zhang, B.; Yin, J.; Huang, L.; Wen, X.; Yang, Y. et al. Tailoring Pt Locations in KL Zeolite by Improved Atomic Layer Deposition for Excellent Performance in n-Heptane Aromatization. *J. Catal.* **2018**, *365*, 163–173.

(49) Injongkol, Y.; Khemthong, P.; Yodsin, N.; Wongnongwa, Y.; Sosa, N.; Youngjan, S.; Butburee, T.; Rungtaweevoranit, B.; Kiatphuengporn, S.; Wittayakun, J. et al. Combined in Situ XAS and DFT Studies on the Role of Pt in Zeolite-Supported Metal Catalysts for Selective n-Hexane Isomerization. *Fuel* **2022**, *314*, 123099.

(50) Schweitzer, J.-M.; Rey, J.; Bignaud, C.; Bučko, T.; Raybaud, P.; Moscovici-Mirande, M.; Portejoie, F.; James, C.; Bouchy, C.; Chizallet, C. Multiscale Modeling as a Tool for the Prediction of Catalytic Performances: The Case of n-Heptane Hydroconversion in a Large-Pore Zeolite. *ACS Catal.* **2022**, *12*, 1068–1081.

(51) Soler, J. M.; Artacho, E.; Gale, J. D.; García, A.; Junquera, J.; Ordejón, P.; Sánchez-Portal, D. The SIESTA Method for Ab Initio Order-N Materials Simulation. *J. Phys. Conden. Matter* **2002**, *14*, 2745–2779.

(52) Perdew, J. P.; Burke, K.; Wang, Y. Generalized Gradient Approximation for the Exchange-Correlation Hole of a Many-Electron System. *Phys. Rev. B* **1996**, *54*, 16533–16539.

(53) Bertini, M.; Ferrante, F.; Duca, D. Empathes: A General Code for Nudged Elastic Band Transition States Search. *Comput. Phys. Commun.* **2022**, *271*, 108224.

Table 1: Numbers of structures following the application of the three sieves characterizing the systems with one, two and three platinum atoms.

	Starting structures	**Structures after**		
		1st **sieve**[a]	**2**nd **sieve**[a]	**3**rd **sieve**[a,b]
Pt$_1$@BEA	683	14	8	4
Pt$_2$@BEA	10, 19, 61, 58	40	3, 4, 3, 2	5
Pt$_3$@BEA	17, 18, 17, 17, 29	20	2, 3, 2, 4, 3	–

[a] For details on the procedure summarized by the term "sieve" see text and Scheme 1

[b] The third sieve selects the m most stable structures with n Pt atoms and allow one to pick out m sets of new starting structures containing $n+1$ Pt atoms. For example, after having applied the third sieve to the Pt$_1$@BEA case, four geometries are left, which can be labeled a, b, c, d; a second Pt atom is added to each of these, so that 148 starting structures are builded for the Pt$_2$@BEA system, *i.e.* 10 structures originating from a, 19 structures from b, 61 from c and 58 from d.

Table 2: ΔE values related to the processes represented by equations (1)-(3), calculated for every investigated BEA cavity investigated.

Structure	**Process ΔE (kJ mol^{-1})**		
	step 1	**step 2**	**step 3**
t-bet(a)	-16.2	+8.6	+24.8
t-bet(b)	-16.2	+18.1	+34.3
t-bet(c)	-16.2	+32.6	+48.8
t-bea-1*(a)	-70.8	-143.3	-72.5
t-bea-1*(b)	-70.8	-116.7	-45.9
t-mtw(a)	-119.8	-101.7	+18.1
t-mtw(b)	-110.3	-207.0	-96.7
t-mtw(c)	-104.3	-242.2	-137.9

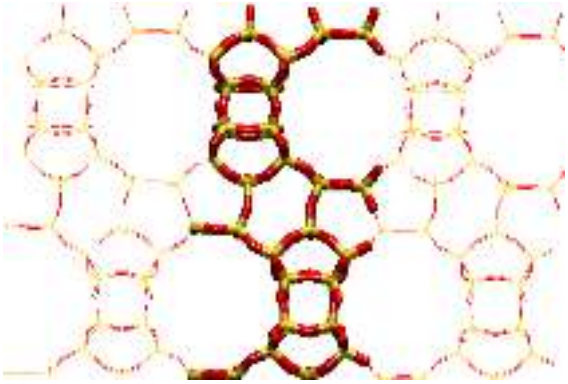

Figure 1: The BEA unit cell of 192 atoms (licorice representation; O=red, Si=yellow), within the periodic framework (wired representation), viewed along the ac plane. The used cell parameters are: a=b= 12.631 Å, c=26.186 Å; $\alpha = \beta = \gamma = 90^{\circ}$.

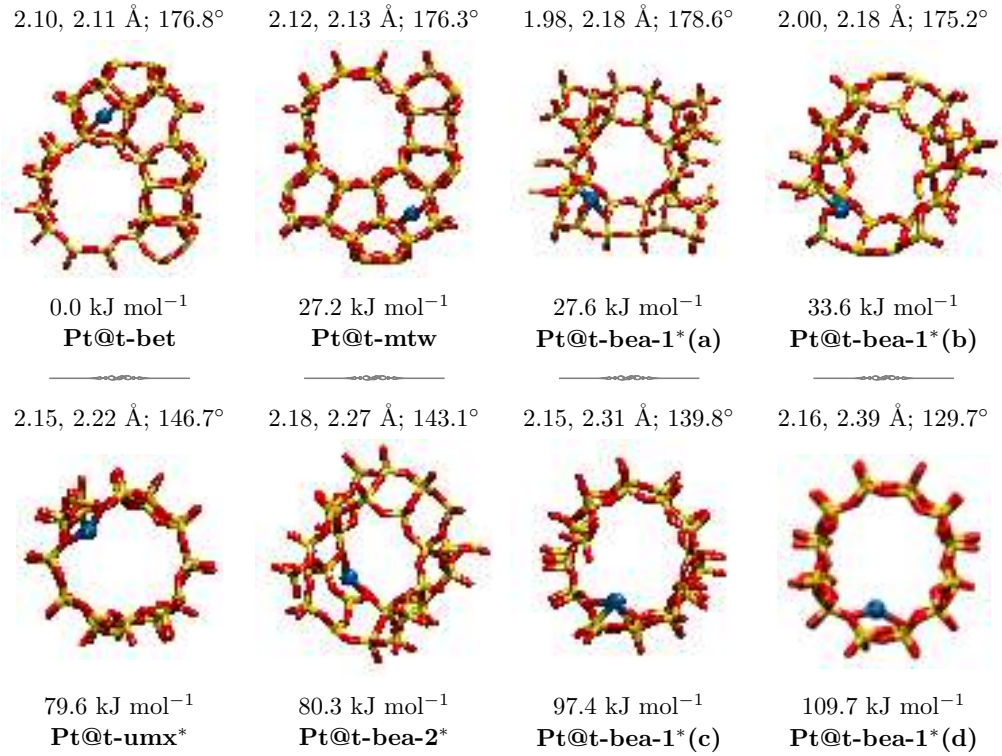

Figure 2: Local views of the eight Pt@BEA optimized geometries (O=red, Si=yellow, Pt=blue). Relevant Pt−O distances and O−Pt−O angles are reported above each structure; below the relative energy values, calculated with respect to the more stable species are also reported along with the tiling arrangement labels used to identify, in accordance with IZA,[13] the cavity in which the platinum atom is located.

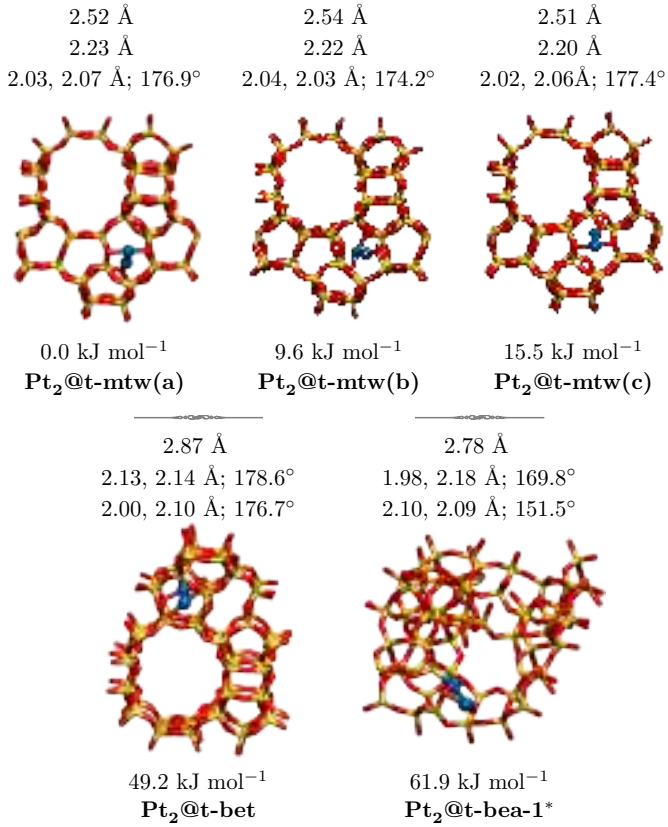

Figure 3: Local views of the five Pt_2@BEA optimized geometries (O=red, Si=yellow, Pt=blue). Above each structure Pt−Pt bond distance is reported, together with relevant Pt−O distances and O−Pt−O angles for the first and the second embedded Pt atom. Below there are the relative energy values, calculated with respect to the most stable species, along with the label used to identify the systems, underlying the cavity in which the first platinum atom is located.

2.56, 2.57, 2.72 Å 58.1°, 64.1°, 57.7° 2.22 Å 2.03, 2.03 Å; 173.9° 2.21 Å	2.88, 2.56, 2.55 Å 55.5°, 68.2°, 55.8° 2.21 Å 1.96, 2.18 Å; 174.5° 2.38 Å	2.94, 2.59, 2.67 Å 54.8°, 67.8°, 83.0° 2.13, 2.01 Å; 165.7° 2.09, 2.16 Å; 148.1° 2.56 Å	2.52, 2.56 Å 171.4° 2.36 Å 2.03, 2.07 Å; 171.9° 2.02 Å
			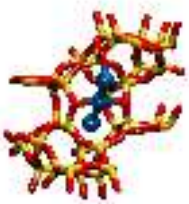
0.0 kJ mol^{-1} **Pt$_3$@t-mtw(c)**	35.2 kJ mol^{-1} **Pt$_3$@t-mtw(b)**	118.2 kJ mol^{-1} **Pt$_3$@t-bea-1*(a)**	140.5 kJ mol^{-1} **Pt$_3$@t-mtw(a)**
2.77, 2.44 2.59 Å 54.0°, 59.1°, 66.7° 1.99, 2.20Å; 167.0° 2.21 Å -	2.77, 2.62 Å 85.1° 2.12, 2.15Å; 172.4° 1.98, 2.14Å; 172.3° 2.09 Å	2.77, 2.63 Å 86.4° 2.12, 2.14Å; 172.7° 1.99, 2.15Å; 174.3° 2.08 Å	2.76, 2.58 Å 88.6° 2.15, 2.18Å; 170.7° 1.99, 2.15Å; 172.1° 2.07 Å
		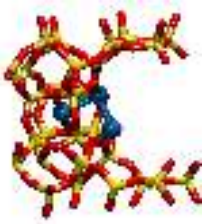	
144.8 kJ mol^{-1} **Pt$_3$@t-bea-1*(b)**	169.1 kJ mol^{-1} **Pt$_3$@t-bet(a)**	178.1 kJ mol^{-1} **Pt$_3$@t-bet(b)**	193.1kJ mol^{-1} **Pt$_3$@t-bet(c)**

Figure 4: Local views of the eight Pt_3@BEA optimized geometries. O=red, Si=yellow, Pt=blue. Above each structure Pt−Pt distances and angles are reported, together with relevant Pt−O distances and O−Pt−O angles for the first, second and third embedded Pt atom. The relative energy values, calculated with respect to the most stable species, are shown below each structure, together with the tiling label identifying the cavity where the first platinum is located.

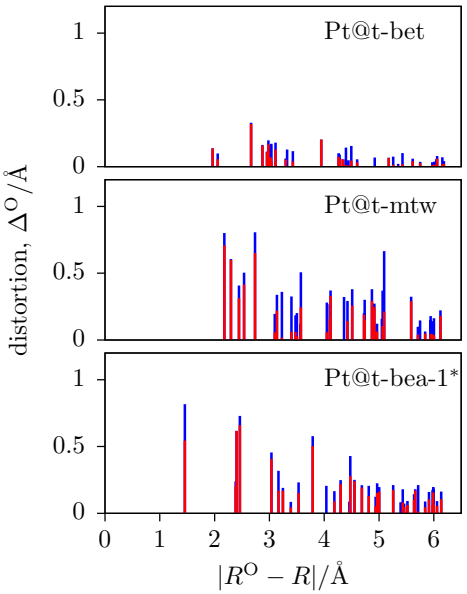

Figure 5: Absolute (Δ_a^{O}, blue) and radial (Δ_r^{O}, red) displacements of the framework oxygen atoms in Pt@BEA systems with respect to the pristine zeolite structure, within an exploration radius of 6.2 Å around the coordinates of the reference point R. Panels of the different cavities in which the platinum atom is located are reported in increasing relative energy, from top to bottom.

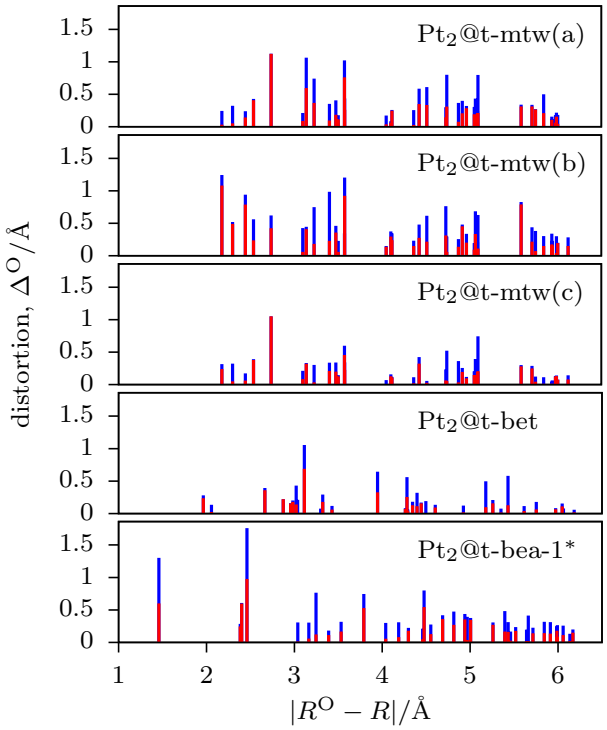

Figure 6: Absolute (Δ_a^{O}, blue) and radial (Δ_r^{O}, red) of the framework oxygen atoms in Pt_2@BEA systems with respect to the pristine zeolite structure, within an exploration radius of 6.2 Å around the coordinates of the reference point R. Panels of the different cavities in which the platinum dimer is located are reported in increasing relative energy, from top to bottom.

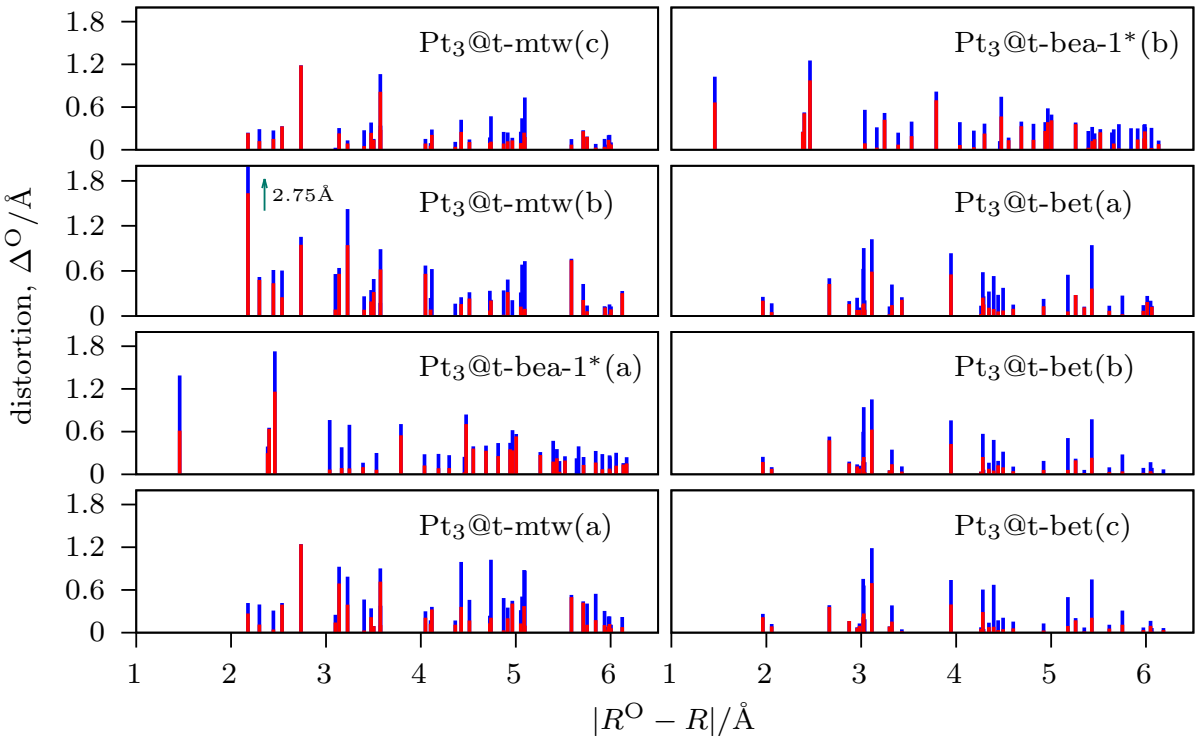

Figure 7: Absolute (Δ_a^{O}, blue) and radial (Δ_r^{O}, red) of the framework oxygen atoms in Pt_3@BEA systems with respect to the pristine zeolite structure, within an exploration radius of 6.2 Å around the coordinates of the reference point R. Panels of the different cavities in which the platinum cluster is located are reported in increasing relative energy, from top to bottom, left to right. The arrow in the Pt_3@t-mtw(b) panel indicates an off-scale point at $\Delta_a^{\mathrm{O}} = 2.75$ Å.

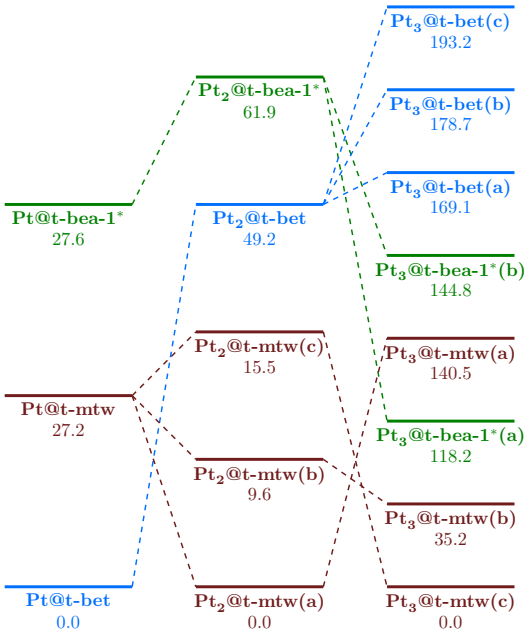

Figure 8: Energetics of and relations between the Pt_n@BEA systems considered for evaluating the clustering tendency. Vertically, cases with 1, 2 and 3 platinum atoms inside the different cavities are reported (left to right). The relative energy within the group is given below the cavity label. Horizontally, cases with the metal atoms in a certain cavity (t-bet-, t-mtw and t-bea-1*, represented by different colors) are connected to their parent Pt_{n-1} system by dashed lines.

TOC Graphic